

From Radio to TeV: The surprising Spectral Energy Distribution of AP Librae

D.A. Sanchez,^{1*} B. Giebels,² P. Fortin,³ D. Horan,² A. Szostek,⁴ S. Fegan,²
A.-K. Baczko,^{5,6} J. Finke,⁷ M.L. Kadler,⁶ Y.Y. Kovalev,^{8,9} M.L. Lister¹⁰ A.B. Pushkarev^{11,12,9}
T. Savolainen^{13,9}

¹Laboratoire d'Annecy-le-Vieux de Physique des Particules, Université de Savoie, CNRS/IN2P3, F-74941 Annecy-le-Vieux, France

²Laboratoire Leprince-Ringuet, Ecole Polytechnique, CNRS/IN2P3, F-91128 Palaiseau, France

³Fred Lawrence Whipple Observatory, Harvard-Smithsonian Center for Astrophysics, Amado, AZ 85645, USA

⁴Kavli Institute for Particle Astrophysics and Cosmology, Department of Physics and SLAC National Accelerator Laboratory, Stanford University, Stanford, CA 94305, USA ⁵Dr

⁶Lehrstuhl für Astronomie, Universität Würzburg, Campus Hubland Nord, Emil-Fischer-Strasse 31, 97074, Würzburg, Germany

⁷U.S. Naval Research Laboratory, Code 7653, 4555 Overlook Ave. SW, Washington, DC, 20375-5352

⁸Astro Space Center of Lebedev Physical Institute, Profsoyuznaya 84/32, 117997 Moscow, Russia

⁹Max-Planck-Institut für Radioastronomie, Auf dem Hügel 69, 53121 Bonn, Germany

¹⁰Department of Physics, Purdue University, West Lafayette, IN 47906, USA

¹¹Crimean Astrophysical Observatory, 98409 Nauchny, Crimea, Russia

¹²Pulkovo Observatory, Pulkovskoe Chaussee 65/1, 196140 St. Petersburg, Russia

¹³Aalto University Metsähovi Radio Observatory, Metsähovintie 114, 02540 Kylmälä, Finland

24 October 2018

ABSTRACT

Following the discovery of high-energy (HE; $E > 10$ MeV) and very-high-energy (VHE; $E > 100$ GeV) γ -ray emission from the low-frequency-peaked BL Lac (LBL) object AP Librae, its electromagnetic spectrum is studied over 60 octaves in energy. Contemporaneous data in radio, optical and UV together with the (non simultaneous) γ -ray data are used to construct the most precise spectral energy distribution of this source. The data have been found to be modeled with difficulties with single zone homogeneous leptonic synchrotron self-Compton (SSC) radiative scenarios due to the unprecedented width of the high-energy component when compared to the lower-energy component. The two other LBL objects also detected at VHE appear to have similar modeling difficulties. Nevertheless, VHE γ rays produced in the extended jet could account for the VHE flux observed by H.E.S.S.

Key words: gamma rays: observations – Galaxies : active – Galaxies : jets – BL Lacertae objects: individual objects: AP Librae

1 INTRODUCTION

Blazars are among the most energetic objects in the Universe that exhibit non-thermal electromagnetic spectra from radio up to very-high-energy (VHE, $E > 100$ GeV) γ -rays, with a two-component spectral energy distribution (SED) structure in a $\nu f(\nu)$ representation. Multi-wavelength data are of paramount importance to understand the mechanisms at play in the jet.

Blazars are divided into two classes: flat spectrum radio quasars (FSRQs) and BL Lacertae (BL Lac) objects, the latter being sub-divided into high-frequency-peaked BL Lac (HBL) and low-frequency-peaked BL Lac (LBL). The distinction between HBL and LBL classes is based on the low-energy peak position (Padovani & Giommi 1995). HBL objects present a peak in the UV

or X-ray range while the peak of LBL objects is located at lower energies (i.e., in optical wavelengths).

So far, the vast majority of BL Lac objects detected in VHE belong to the HBL sub-class¹. The SEDs of HBL objects are often successfully modeled with a synchrotron self-Compton (SSC) model, in which the low-energy emission is produced by synchrotron radiation of relativistic electrons, and the high-energy component by inverse Compton scattering off the same synchrotron photons. HBL are the dominant class of extragalactic objects detected by ground-based Atmospheric Čerenkov Telescopes (ACTs) in the TeV γ -ray regime.

Only a few TeV emitters belong to the LBL sub-class and, among them, AP Librae ($z = 0.049$, Jones et al. 2009) was recently

* david.sanchez@lapp.in2p3.fr

¹ To keep track of the number of detected object, an up-to-date VHE γ -ray catalogue can be found in the TeVcat <http://tevcat.uchicago.edu>

detected by the H.E.S.S. collaboration (Abramowski et al. 2015) with a flux of $8.78 \pm 1.54_{\text{stat}} \pm 1.76_{\text{sys}} \times 10^{-12} \text{ cm}^{-2} \text{ s}^{-1}$ above 130 GeV and a photon index $\Gamma = 2.65 \pm 0.19_{\text{stat}} \pm 0.20_{\text{sys}}$ matching well the spectrum measured by the *Fermi* Large Area telescope (LAT) in the high energy (HE, 100 MeV < E < 300 GeV) range. Remarkably, the spectral break between the HE and VHE ranges is the smallest ever measured for an LBL object but cannot be explained by extragalactic background light (EBL) attenuation only (Sanchez et al. 2013). In this work, VHE and HE data have been extracted from Abramowski et al. (2015)

After the announcement of this detection by the H.E.S.S. collaboration (Hofmann 2010), *Swift* and *RXTE* data were taken creating contemporaneous spectra in X-ray and UV bands. Analysis and results are presented in sections §2.1 and §2.3. Archival observation by *Chandra* (§2.2) have been analyzed in this work, revealing the first X-ray extended jet for a VHE blazar. At longer wavelengths, AP Librae is one of the targets of different monitoring programs such as SMARTS (§2.3) and the MOJAVE program (§2.4) which provide long-term optical and VLBA measurements. The VHE detection, together with lower energy-data presented in this paper, enable to draw the first complete SED of this source and to probe mechanisms at play in LBL objects. The broadband SED is then discussed in the framework of different emission models in §3.

Throughout this paper a Λ CDM cosmology with $H_0 = 71 \text{ km s}^{-1} \text{ Mpc}^{-1}$, $\Omega_\Lambda = 0.73$ and $\Omega_M = 0.27$ is assumed, resulting in a luminosity distance for AP Librae of $D_L = 215 \text{ Mpc}$ and a linear scale of 0.947 kpc per arcsecond (Wright 2006).

2 MULTI-WAVELENGTH OBSERVATIONS

2.1 *Swift*-XRT and *RXTE*-PCA observations

X-ray observations of AP Librae during the period of interest were retrieved using the HEASARC archive. Four consecutive daily observations (ObsID 95141) of $\approx 3 \text{ ks}$ each were carried out between 10–14 July 2010 with *RXTE* (Jahoda et al. 1996), with a total exposure of $\approx 13 \text{ ks}$. The STANDARD2 *RXTE*-PCA data were extracted using the ftools in the HEASOFT 6.16 software package provided by NASA/GSFC and filtered using the *RXTE* Guest Observer Facility recommended criteria. Only signals from the top layer (X1L and X1R) of Proportional Counter Unit 2 (PCU2) were used to extract spectra in the 3 – 50 keV range, using the faint-background model. The obtained daily light curve has an average rate of 0.44 counts s^{-1} , a variance of 0.03 counts s^{-2} compatible with its expected variance of 0.02 counts s^{-2} if the source were constant, and a chi-square probability of constancy of 27%, hence no variability is present over the span of 4 days.

During the period of interest, seven observations were carried out by the *Swift* mission (Burrows et al. 2005), between 20 February 2010 and 16 August 2011 (ObsID 36341005 to 36341011), of which one 5 ks observation was carried out on 7 July 2010, near the *RXTE* observation. However, the short observation in ObsID 36341009 was skipped. The photon-counting (PC) mode data are processed with the standard *xrtpipeline* tool (HEASOFT 6.16), with the source and background-extraction regions defined as a 20-pixel (4.7 arcsec) and a 40-pixel radius circle respectively, the latter being centered nearby the former without overlapping. All exposures show a source with a stable average count rate of $\approx 0.12 \text{ counts s}^{-1}$. Also the large 5 ks XRT-PC light curve shows the source with an average count rate of $(0.13 \pm 0.02) \text{ s}^{-1}$ and

an r.m.s. of $\approx 0.01 \text{ s}^{-1}$ for which no variability could be found with a 99% confidence level upper limit on the fractional variance (as defined in Vaughan et al. 2003) F_{var} of 0.95. Using this count rate in WebPIMMS from HEASARC, a *RXTE*-PCA count rate of $\approx 0.6 \text{ counts s}^{-1}$ is predicted, compatible with the value actually observed of 0.44 counts s^{-1} hinting at the fact that the source was probably in the same state during observations of both observatories. Given the low count rate, no pile-up is expected in PC mode, which is confirmed by the acceptable fit of a King profile to the PSF of all observations.

Spectral fitting of all ObsIDs was performed with PyXspec v1.0.4 (Arnaud 1996), using a response matrix for the combined PCA data set generated by the ftool *pcarsp* v11.7.1, and dedicated Ancillary Response Functions (ARFs) for all XRT data sets generated by *xrtmkarf* (along with the latest spectral redistribution matrices *swxpc0to12s6_20110101v014* from CALDB). Spectra from all ObsIDs were rebinned to have at least 20 counts per bin using *grppha*, channels 0 to 29 were ignored in the XRT-PC data, and only the 3–50 keV range is used in the PCA data. All data sets are fit to a power-law model $dN/dE = N_0(E/E_0)^{-\Gamma_X}$, where N_0 is the normalization factor at a chosen reference energy $E_0 = 1 \text{ keV}$ and Γ_X the photon index. Using the Leiden/Argentine/Bonn (LAB) Survey of Galactic HI (Kalberla et al. 2005) weighted average hydrogen column density of $N_{\text{H}} = 8.14 \times 10^{20} \text{ cm}^{-2}$, good fits are obtained for the power-law function ($P(\chi^2) = 0.18 - 0.9$) with a photon index of $\Gamma_X \approx 1.55$ on average. All XRT observations were also summed, a new exposure file built with *ximage*, and a new ARF for the summed spectrum. This latter spectrum extends up to $\approx 7 \text{ keV}$. Another spectrum was derived this time limited to 1 count/bin, to allow an extension to higher energies, and was fitted using *statistic cstat* required in the case of Poisson data. The fit parameters are entirely compatible with those obtained using χ^2 statistics, but the spectrum extends up to $\approx 10 \text{ keV}$. All fit parameters, along with the unabsorbed 0.3–10 keV flux $F_{0.3-10 \text{ keV}}$ (retrieved for each flux using *cflux*), are shown in Table 1 and the light curve is shown on Figure 1.

Systematic errors on the *Swift*-XRT spectra and absolute flux are less than 3% and 10%, respectively (Godet et al. 2009), while PCA-XRT cross-calibration details can be found in Tsujimoto et al. (2011).

2.2 *Chandra* observations

AP Librae was observed by *Chandra* on July 4, 2003 with a total exposure time of 14 ks. The *Chandra* data reprocessing and reduction were performed following the standard procedures described in the *Chandra* Interactive Analysis of Observations² (CIAO) threads, using CIAO v4.3 and the *Chandra* Calibration Database (CALDB) version 4.4.6. The data reveal the presence of an extended jet on arcsecond scales, which is unique amongst the VHE emitting BL Lac class so far. A radio VLA observation was used to align the nuclear X-ray emission with the radio core. A registered, exposure-corrected and adaptively smoothed image of AP Librae in units of $\text{ph cm}^{-2} \text{ s}^{-1} \text{ px}^{-1}$, with radio contours overlaid is shown in Figure 2. In order to assess to what degree the *RXTE* and *Swift* spectra need corrections for non-core emission, the spectrum of the jet is estimated, with the caveat that this observation is not contemporaneous with the data set presented here.

² <http://xc.harvard.edu/ciao/index.html>

Table 1. Results of the spectral fitting of all XRT-PC and PCA observations

ObsID	Time MJD-5500	N_0 $\text{ph cm}^{-2} \text{s}^{-1}$	Γ_X	$P(\chi^2)$ %	$F_{0.3-10\text{keV}}$ $\times 10^{-12} \text{ erg cm}^{-2} \text{ s}^{-1}$
00036341005	247.2-247.2	$(9 \pm 1) \times 10^{-4}$	1.62 ± 0.14	18	6.8 ± 0.8
00036341006	249.5-249.7	$(9 \pm 1) \times 10^{-4}$	1.45 ± 0.09	70	7.6 ± 0.6
00036341007	384.7-384.8	$(8.3 \pm 0.4) \times 10^{-4}$	1.47 ± 0.06	31	7.2 ± 0.4
00036341008	608.1-608.2	$(10 \pm 1) \times 10^{-4}$	$1.49^{+0.15}_{-0.14}$	35	$8.3^{+1.0}_{-0.9}$
00036341010	608.0-608.0		1.51 ± 0.09	94	7.8 ± 0.6
00036341011	609.8-609.9	$(9.3 \pm 0.5) \times 10^{-4}$	$1.52^{+0.07}_{-0.06}$	60	7.6 ± 0.4
sum all above		$(9.2 \pm 0.2) \times 10^{-4}$	1.52 ± 0.02	99	7.54 ± 0.2
95141	387.9-391.9	$1.3^{+0.4}_{-0.3} \times 10^{-3}$	1.74 ± 0.16	91	5.6 ± 0.4

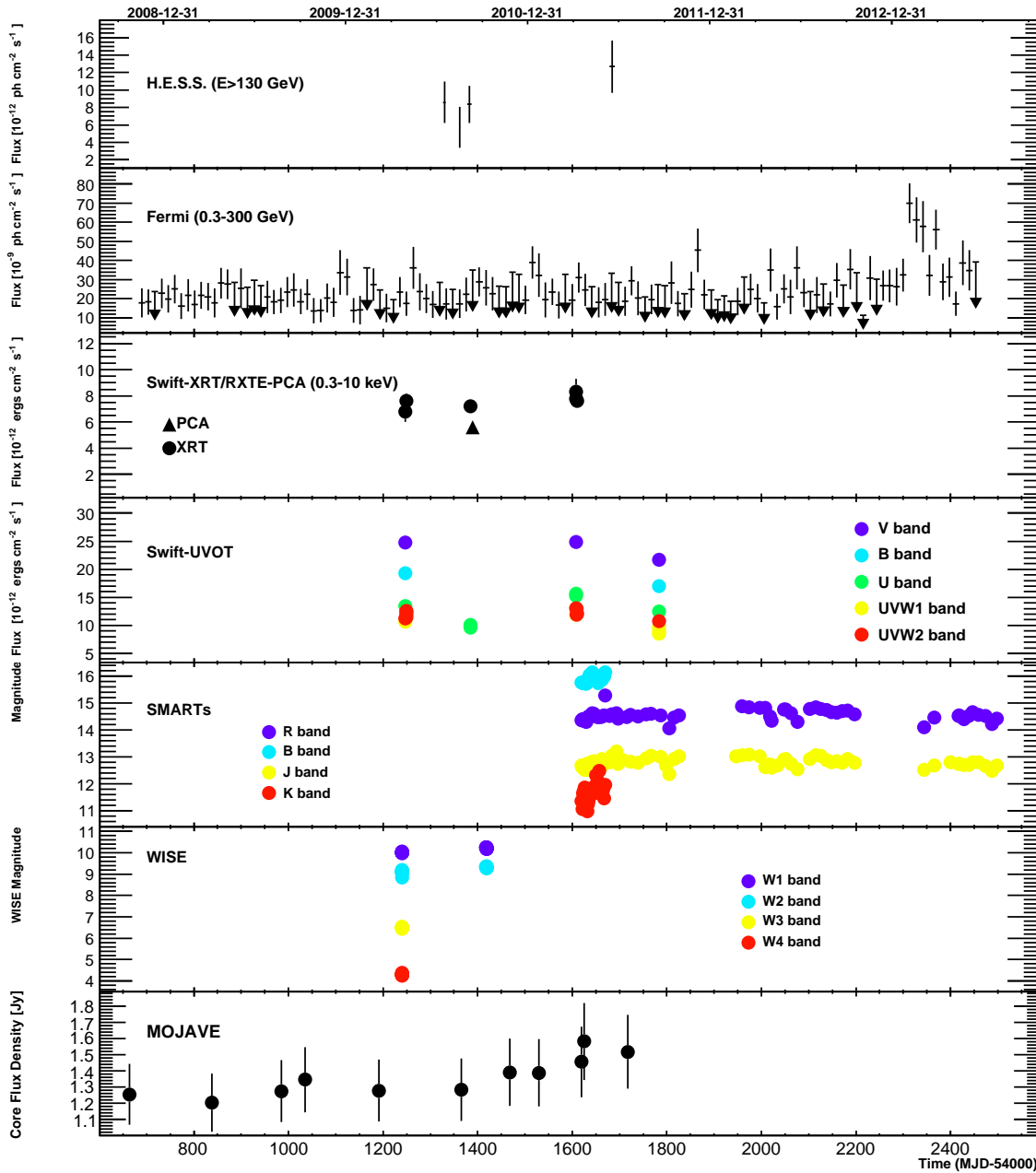


Figure 1. Light curves of AP Librae in, from top to bottom, VHE, HE, X-rays, UV, Optical and radio (15 GHz) wavebands. The 4 RXTE observations (ObsID 95141) were merged together and the seven *Swift* observations (ObsID 36341005 to 36341011) are shown individually.

A spectrum of the jet was taken from a polygon shaped region which avoids the emission of the core and the ACIS readout streak. A core spectrum comes from a 2 arcsecond region centered on the core. A background spectrum was extracted from four circular regions placed to the north and south of the source. The jet and background regions are marked in Figure 2. In order to estimate the effects of pile-up in the core and jet region, the method described by Harris et al. (2011) was used. In the jet region no pile-up was found while it was necessary to correct for mild pile-up in the core.

The spectra of the core and the jet contain ≈ 4900 and ≈ 200 background subtracted counts, respectively. Both spectra were binned to a minimum of 20 counts per bin, and fit in the 0.5–7.0 keV energy band using an absorbed power-law model in XSPEC with the same N_{H} as in §2.1. The fit of the jet spectrum yields a photon index $\Gamma_{\text{jet}} = 1.59 \pm 0.16$ and a 2–10 keV unabsorbed flux of $F_{2-10\text{keV}}^{\text{jet}} = (1.07 \pm 0.37) \times 10^{-13}$ erg cm $^{-2}$ s $^{-1}$, with a $\chi^2 = 4.4$ for 7 dof, or more than an order of magnitude below the value measured for the source in §2.1 based on the *Swift* and *RXTE* data, which can hence safely be used as the X-ray flux of the core in AP Librae. The jet spectrum is comparable with the spectra of large-scale quasar jets observed by *Chandra*, which may also be sources of relatively intense γ -ray emission (see the discussion in Sambruna et al. 2004; Finke et al. 2008). Such a scenario is not formally excluded here since an extrapolation of the jet spectrum could connect within the experimental errors with either the HE or VHE fluxes reported here. Assuming no pile-up, the best power-law fit to the core spectrum yields a photon index of $\Gamma_{\text{core}} = 1.51 \pm 0.03$ and a 2–10 keV unabsorbed flux of $F_{2-10\text{keV}}^{\text{core}} = 3.18^{+0.19}_{-0.14} \times 10^{-12}$ erg cm $^{-2}$ s $^{-1}$. Using the pileup model in XSPEC, a pile-up corrected spectrum appears however to be softer with $\Gamma_{\text{core}} = 1.68^{+0.03}_{-0.06}$ and $F_{2-10\text{keV}}^{\text{core}} \approx 2.31 \times 10^{-12}$ erg cm $^{-2}$ s $^{-1}$, with a $\chi^2 = 158.4$ for 129 dof. The pile-up model of Davis (2001) was used in the fit of the core spectrum, and the value of the pile-up parameter $\alpha > 0$ indicates that the fit is indeed affected by this. However, it was not possible to obtain an error estimate on α , and hence we also do not have an error estimate on the unabsorbed and pile-up corrected flux. Due to pile-up effects, the fit results for the core should be treated with caution. This extended X-ray jet was first reported by Kaufmann et al. (2013). Our results differ slightly, probably because we used different extraction and background regions, and Kaufmann et al. did not take into account the above-mentioned ACIS readout streak.

2.3 *Swift*-UVOT and SMARTS observations

All of the available archival data taken on AP Librae with the ultraviolet and optical telescope (UVOT) on the *Swift* satellite were analyzed. This comprised 35 exposures taken between April 2007 and July 2010, 13 of which occurred during the time frame with which this paper is concerned (see Figure 1). After extracting the source counts from an aperture of 5.0'' radius around AP Librae and the background counts from four neighboring regions, each of the same size, the magnitudes were computed using the *uvotsource* tool with calibrations from Breeveld et al. (2011). These were converted to fluxes using the values from Poole et al. (2008) after correction for extinction following the procedure and R_v value of Roming et al. (2009). The values of a and b from Roming et al. (2009), computed following the procedure of Cardelli et al. (1989), were used. The $E(B - V)$ value from Schlafly & Finkbeiner (2011), accessed through the NASA/IPAC Extragalactic Database, was used. Results are summarized in Table 2.

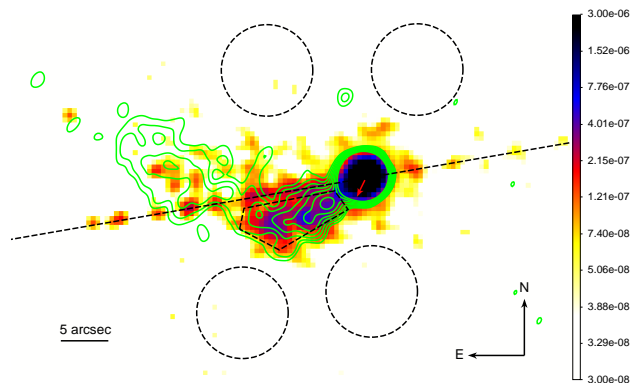


Figure 2. Adaptively smoothed, exposure corrected X-ray image obtained by *Chandra* in the 0.5–7 keV energy band in units of ph cm $^{-2}$ s $^{-1}$ px $^{-1}$ with the pixel size of 0.492'', where one arcsecond corresponds to 0.947 kpc on linear scale. Overlaid are 1.4 GHz radio emission contours at 2'' resolution from reprocessing archival VLA data (program AB700; C.C. Cheung, private communication). The flux densities of radio contours increase by a factor of 1.5, starting from a value of 5 times the rms noise equal to 1.82×10^{-4} Jy beam $^{-1}$. The small red arrow in the radio core shows the orientation of the milliarcsecond scale radio jet seen in VLBA (see e.g. Lister et al. 1998; Zensus et al. 2002), and references therein, for a discussion on the radio jet at different scales). A black dashed polygon delimits the region used to calculate the jet spectrum, the dashed circles are the background regions and a black dashed line indicates a location of an ACIS readout streak.

AP Librae was observed in context of the Yale *Fermi*/SMARTS project³ (Bonning et al. 2012). Observations were performed in the B, R, J and K bands between February 27, 2011 (MJD 55619) and March 3st, 2013 (MJD 56739) and shown on Figure 1. The number of observations and the mean magnitudes are given in Table 2 together with the corresponding fluxes. Magnitudes have been corrected for Galactic absorption using values from Schlafly & Finkbeiner (2011) and converted in flux units using the Bessell zero points (Bessell 1990).

The host galaxy of AP Librae is bright and therefore the contribution from starlight must be taken into account to estimate the non-thermal flux from the core in the near-infrared to UV band. The dereddened near-infrared and optical measurements of AP Librae reported in Figure 1 of Falomo et al. (1993), where the total emission was modeled with a giant elliptical galaxy template and a superposed non-thermal power-law continuum, are given for illustration in the composite SED of Figure 3. The synchrotron emission probably peaks in the optical- to near-IR range, since the spectral index for AP Librae in that range is $\alpha_{\text{IROP}} = 0.95 \pm 0.10$. In Hyvönen et al. (2007), the fluxes in the B and U bands were calculated for the host galaxy and the core. The fractional contribution of the latter was $\approx 42\%$ in the B band and $\approx 69\%$ in the U band. At higher energies the emission from the core accounts for an even higher percentage. To take this result into account, the host galaxy template of Silva et al. (1998) has been used and with a normalization adjusted to fit the data.

2.4 MOJAVE

The parsec-scale structure of the radio jet of AP Librae has been monitored throughout the past decade as part of the MOJAVE pro-

³ <http://www.astro.yale.edu/smarts/glast/pubs.html>

Table 2. Summary of the *Swift*-UVOT and SMARTS results. Columns 1 and 3 give the filter and corresponding energies and the second column gives the number of observations. Magnitudes (column 4) are not corrected for Galactic absorption. The last column gives the corrected flux.

Filter	N_{Obs}	Energy [eV]	magnitude	Flux [10^{-11} erg cm^{-2} s^{-1}]
SMARTS:				
K	25	0.56	11.63±0.37	1.96±0.78
J	79	0.99	12.76±0.17	3.26±0.54
R	74	1.77	14.53±0.18	1.88±0.34
B	29	2.86	15.85±0.13	1.35±0.18
<i>Swift</i> -UVOT:				
V	3	2.30	15.18 ± 0.04	2.43 ± 0.10
B	3	2.86	15.94 ± 0.04	1.69 ± 0.06
U	7	3.54	15.68 ± 0.04	0.96 ± 0.03
UVW1	6	4.72	15.88 ± 0.05	0.63 ± 0.03
UVW2	10	6.12	16.12 ± 0.05	0.57 ± 0.02
UVM2	3	5.57	16.09 ± 0.06	0.55 ± 0.03

gram⁴ (Monitoring of Jets in Active galactic nuclei with VLBA Experiments) with the Very Long Baseline Array (VLBA) at a frequency of 15 GHz. The VLBA data have been calibrated and analyzed following the procedures described by Lister et al. (2009). The source shows a bright, continuous inner jet region with a bright jet core, i.e. apparent jet base, extending towards the South. At a resolution of typically $\approx (1.5 \times 0.5)$ milli-arcsecond (mas), the core is not clearly separated from the inner jet. Elliptical Gaussian components were used to model the brightness distribution and to determine radio flux densities of different emission regions within the source. For the comparison with higher-energy multiwavelength data, we focused on the inner 1.5 mas (≈ 1.41 pc) region, which could typically be modeled with 2–3 Gaussian model components. We have used different models with circular and elliptical model components and tested the formal statistical model-fitting uncertainties of the total flux density, which turn out to be much smaller ($\lesssim (1 - 3)\%$) than the absolute calibration uncertainty, which can be conservatively estimated to be of the order of $\lesssim 10\%$.

The 16 MOJAVE observations from MJD 53853 to 55718 do not show sign of significant variability in the VLBI core region. Figure 3 shows the value of 1.48 Jy of the radio flux density, averaged over the full observations, from the inner 1.5 mas jet core.

3 DISCUSSION

3.1 The radiative components

The composite SED of AP Librae is shown in Figure 3. Together with the MOJAVE, SMARTS, *Chandra*, *Swift*-UVOT, *Swift*-XRT, *RXTE*, *Fermi*-LAT and H.E.S.S. data analyzed in this work, archival data from NED are reported. In the 30–353 GHz band, the *Planck* measurements from the Early Release Compact Source Catalog (ERCSC, Planck Collaboration et al. 2011) are in good agreement with the archival data as are the Wide-field Infrared Survey Explorer (WISE, Wright et al. 2010) data in the bands 3.4, 4.6, 12, and 22 μm .

An extrapolation of the hard X-ray to the optical-UV power-law spectrum reported here underestimates the simultaneous UVOT flux by at least 2 orders of magnitude, though the steeply falling UV spectrum possibly connects with the onset of the XRT spectrum. This indicates the presence of an inflection point in the SED widely attributed to a transition from synchrotron to IC dominated radiation. This feature shows that the Compton component of AP Librae is the broadest ever observed in any blazar, spanning more than 10 decades in energy from ≈ 0.1 keV to ≈ 1 TeV. Indeed, only two other objects of the same class as AP Librae, and hence with broad Compton components, have been detected at VHE energies so far: BL Lacertae ($z = 0.069$), the first LBL object to be proved as being a VHE emitter (Albert et al. 2007), and S5 0716+714 ($z = 0.310$) following an optical trigger (Anderhub et al. 2009). The observed VHE spectrum of the former is not as energetic as AP Librae, and the X-ray spectrum of the latter appears to still belong to the synchrotron component.

An empirical characterization of the two radiative components, through a third degree polynomial fit of each hump in νF_ν representation (as in, e.g., Abdo et al. 2010), is used to estimate the synchrotron and IC peak energies. The values of the parameters obtained from a χ^2 fit⁵ are given in Table 3 and the results are represented in the composite SED of Figure 3. As mentioned above, the SMARTS and the *Swift*-UVOT measurements in the V, B and U were not used in the fit of the synchrotron peak as well as the data from Falomo et al. (1993). The position of the synchrotron peak is then estimated to be $E_{s,\text{peak}} \approx 0.18 \pm 0.06$ eV, which is compatible with the value of $E_{s,\text{peak}} = 0.26$ eV derived by Abdo et al. (2010) on a different data set. The same authors estimated $E_{ic,\text{peak}} = 2.6^{+3.2}_{-1.4}$ GeV for AP Librae in Table 13 based on a strong correlation of $E_{ic,\text{peak}}$ with the HE photon index Γ_{HE} , as expressed in their Equation 5⁶. Using the photon index found by Abramowski et al. (2015), which is based on an order of magnitude larger data set, yields a lower but still compatible value of

⁵ The EBL absorption has been taken into account in the fit.

⁶ The quoted uncertainty, not given in their table, is derived from their estimation of an error of 0.7 associated with the estimation of the log of $E_{ic,\text{peak}}$ in Equation 5.

⁴ <http://www.physics.purdue.edu/astro/MOJAVE>

$E_{\text{ic,peak}} = 0.9_{-0.5}^{+1.0}$ GeV and this value was constrained to be below 1 GeV by fitting the HE-VHE data (Abramowski et al. 2015). The polynomial fit presented here yields a much lower value of $E_{\text{ic,peak}} = 17_{-6}^{+24}$ MeV, which can be attributed to use of the entire SED. This is the lowest IC component peak ever measured for a TeV-emitting blazar.

The third degree polynomial also provides a straightforward estimation of the curvatures κ_s and κ_{IC} at the peak positions $E_{s,\text{peak}}$ and $E_{\text{ic,peak}}$, respectively, which pertain to the widths of each hump. Paggi et al. (2009) show that a relation $\kappa_s = 2\kappa_{\text{IC}}$ is expected in a pure Thomson scattering regime, using a logparabolic parametrization of each of the two humps generated by a single zone homogeneous SSC model, while $\kappa_s = \kappa_{\text{IC}}/5$ in the Klein-Nishina (KN) regime. The curvatures found here for AP Librae yield a surprising $\kappa_s \approx 6.6\kappa_{\text{IC}}$, emphasizing the broadness of the IC component compared to the synchrotron hump, which is hardly possible to reproduce with simple radiative models.

3.2 Radiative scenarios

In a one zone homogenous SSC framework, electrons produce synchrotron photons which are upscattered through the IC mechanism by the same electrons to generate the HE and VHE photons. If this upscattering occurs predominantly in the Thomson regime up to the peak energy, then it becomes possible to constrain the product of the magnetic field B and the Doppler factor δ for a single zone homogenous SSC model (following Tavecchio et al. 1998, Equation 4):

$$B\delta = (1+z) \frac{8.6 \times 10^7 E_{s,\text{peak}}^2}{E_{\text{ic,peak}}}, \quad (1)$$

where the peak energies are expressed in eV. Using the range for $E_{s,\text{peak}}$ found previously and $E_{\text{ic,peak}} = 17$ MeV yields $B\delta = 0.17$ G. The value of the break Lorentz factor γ_b of the underlying electron distribution can also be derived from the ratio of the peak emission energies as $\sqrt{\frac{3E_{\text{ic,peak}}}{4E_{s,\text{peak}}}} \approx 8.5 \times 10^3$.

Assuming now that the observed synchrotron radiation does not exceed ≈ 0.1 keV, (i.e. the lowest energy bin in the XRT spectrum), which is more likely to belong to the onset of the IC component, then this constrains the maximal Lorentz factor γ_{max} of the underlying electron population through the maximum synchrotron energy

$$E_{s,\text{max}} \approx \gamma_{\text{max}}^2 \frac{B\delta m_e c^2}{B_{\text{cr}}(1+z)} \leq 0.1 \text{ keV},$$

where $B_{\text{cr}} = 4.414 \times 10^{13}$ G is the critical magnetic field leading to

$$\gamma_{\text{max}} \leq 10^5 B^{-1/2} \delta^{-1/2}. \quad (2)$$

Using Equation 2 and Equation 1 then yields $\gamma_{\text{max}} \leq 2.4 \times 10^5$, which is consistent with being a factor $\sqrt{E_{s,\text{max}}/E_{s,\text{peak}}}$ higher than γ_b as expected.

Supposing that electrons with an apparent energy of $\delta\gamma_{\text{max}}$ have sufficient energy to upscatter photons to at least the maximal observed Compton energy $E_{\text{ic,max}} \approx 1$ TeV, then the Doppler factor is constrained to a reasonable value of $\delta \geq 10$. If the scattering of 0.1 keV photons occurs in the Thomson regime, the Doppler factor should be such that $4\gamma_{\text{max}} \times 0.1 \text{ keV} \leq \delta m_e c^2$. Using the value for γ_{max} found above leads to an unusually high value of $\delta \geq 163$. If however the scattering occurs in the KN regime for these highest energy seed photons, then $E_{\text{ic,max}} = \frac{\delta m_e c^2}{1+z} \gamma_{\text{max}}$ which, combined with the above constraint (Equation 2) on γ_{max} , then yields

$$B\delta^{-1} \leq 2.3 \times 10^{-3} \text{ G}, \quad (3)$$

from which follows, using the above constraint $\delta \geq 10$, a reasonable constraint of $B \leq 2.3 \times 10^{-2}$ G. In Appendix A, similar conclusions are drawn for an arbitrary type of seed photons.

Lister et al. (2013) measured an apparent superluminal motion 6.4c. This is compatible with $\delta > 10$ for a viewing angle below < 5 degrees and with $\delta = 20$ for 1.7 degrees.

Going further by assuming that photons with energies up to $E_{\text{ic,peak}}$ are produced in the Thomson regime, and the ≈ 1 TeV photons in the KN regime, then Equation 1 and Equation 3 can be combined to give $B \leq 2 \times 10^{-2}$ G regardless of the value of δ .

3.3 Application of an SSC model to the SED

The time-averaged SED of AP Librae was modeled with a canonical one zone homogeneous SSC model (Band & Grindlay 1985). A spherical region of size R , with an electron distribution $N_e(\gamma)$, moving with a bulk Doppler factor δ , is filled uniformly with a magnetic field B . As in Tavecchio et al. (2010), $N_e(\gamma)$ is described by a broken power-law of index S_1 between $\gamma = 1$ and γ_b and S_2 between γ_b and γ_{max} . The electrons lose their energy by synchrotron emission, producing a field of photons which become the targets for the same electron population through the IC process. The KN effects are taken into account using the *Jones kernel* (Jones 1968) to compute the IC cross-section.

A tentative model is shown in Figure 3, where the shape of the electron distribution (S_1 , S_2 and γ_b) is constrained by the observed synchrotron component. The remaining parameters (R , B , δ , and the total number of electrons $N_{e,\text{tot}}$) are adjusted to reproduce the onset of the Compton component in the X-rays. The obtained parameters and model curves, as given in Table 4 and Figure 3, respectively (together with the model parameters and curves derived by Tavecchio et al. (2010) for comparison) obey the constraints found in §3.2. Not surprisingly, the broad IC component of the SED is difficult to reconcile with the synchrotron distribution using such a simple model, for which strong indications were already presented in §3.1.

The SSC calculation reproduces well the lower energy part of the SED, up to the X-rays, but the spectral prediction in the *Fermi-LAT* energy range is much softer, as well as about one order of magnitude above the observed HE flux. The direct consequence of the broadness of the IC component is that the H.E.S.S. flux is largely underestimated. Directly linked to the electron distribution and to the well measured synchrotron component, this shape can only be affected by the KN effects, which tend to soften the spectrum leading inevitably to even larger disagreements.

3.4 VHE γ Rays from the extended jet?

As seen in the previous sections, one-zone SSC models cannot reproduce the broadband SED of AP Librae. However, Böttcher, Dermer, & Finke (2008) proposed that the Compton-scattering of the cosmic microwave background (CMB) by electrons in an extended kpc-scale jet could make VHE γ -rays. This model was suggested to explain the hard VHE spectrum from 1ES 1101–232 as observed by H.E.S.S. (Aharonian et al. 2006, 2007), when EBL attenuation was taken into account with the models available at the time. AP Librae has an extended kpc-scale jet resolved in radio (see Figures 3 and 4) and X-rays (see section 2.2), and it has long been thought that the Compton-scattering of CMB photons could produce the X-rays observed from these extended

Table 3. Parameters of third degree polynomial function describing the low and high-energy component of AP Librae. The function is of the form $f(E) = p_0 + p_1 \log_{10}(E/\text{eV}) + p_2 \log_{10}^2(E/\text{eV}) + p_3 \log_{10}^3(E/\text{eV})$

Energy Range (eV)	p_0	p_1	p_2	p_3
$3 \times 10^{-4} - 50$	-10.79	-0.52	-0.41	-0.048
$50 - 10^{13}$	-13.36	0.82	-0.068	-0.001

Table 4. Parameters of the SSC model presented in this work and from Tavecchio et al. (2010). For both models, $\gamma_{\min} = 1$ was used.

Model	γ_b	γ_{\max}	S_1	S_2	$N_{e,\text{tot}}$	B	R	δ
	10^4	10^4			10^{53}	$10^{-2}[\text{G}]$	$10^{16}[\text{cm}]$	
This work	1.1	2.3	2	4.9	5.4	0.9	3.5	20
Tavecchio et al	2.0	5	2	4.9	0.4	1.2	1	40

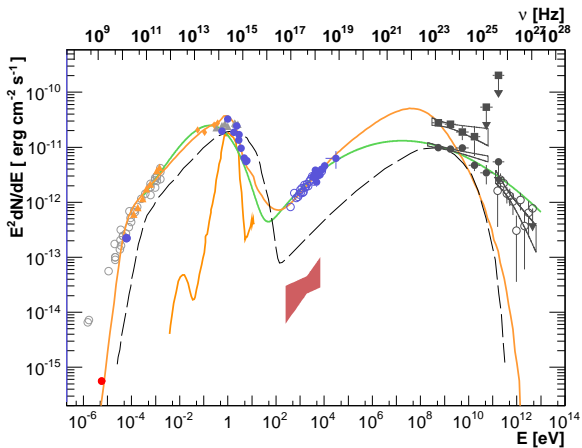


Figure 3. The broadband SED of the LBL AP Librae. The orange triangles come from the *Planck* ERCSC. The orange diamonds are WISE measurements. Blue points are, from low energy to high energy, MOJAVE(15GHz), *Swift*-UVOT (2.30–5.57 eV), SMARTS (0.56–2.86 eV), *Swift*-XRT/RXTE (3–50 keV). Grey points and butterflies are *Fermi*-LAT for the quiet (circle) and flare (square) periods (0.3–300 GeV) and H.E.S.S. ($E > 100$ GeV) measurement from (Abramowski et al. 2015). *Swift*-UVOT, SMARTS data are corrected for Galactic extinction and X-ray data are corrected for N_{H} absorption. Light gray data are taken from NED. The dark gray triangles come from Falomo et al. (1993). The red point is the radio flux of the extended jet. The orange line is the host galaxy template of Silva et al. (1998). The fit with two third degree polynomial functions, not corrected for EBL, are shown with a green line (see §3.1). The red butterfly is the *Chandra* spectrum from the jet. The dashed line is the SSC model from Tavecchio et al. (2010) whereas the red line is the model obtained in this work (see Table 4).

jets (e.g., Tavecchio et al. 2000; Celotti et al. 2001). Therefore, it seems natural to apply this model to AP Librae, to see if the extended jet emission could plausibly make up the VHE γ rays. Thus, the broadband SED of AP Librae has been modeled with a compact, synchrotron/SSC model based on Finke et al. (2008), and an additional component from the extended jet, emitting synchrotron and inverse Compton-scattering of CMB photons (hereafter IC-CMB).

The result of this model is shown in Figure 4, with the model parameters in Table 5. The model parameters are fully described

in Finke et al. (2008). The compact component can explain the radio, optical (not including emission that is clearly from the host galaxy), X-ray, and the lower-energy *Fermi*-LAT γ -ray data. The extended component can explain the extended radio and X-ray data, as well as the highest γ -ray emission detected by the LAT and H.E.S.S. A double-broken power-law was used to describe the electron distribution in the compact component, while only a single broken power-law was needed for the electron distribution in the extended component. Parameters in the compact component are broadly comparable to synchrotron/SSC modeling results for other BL Lac objects, including the jet power in electrons being several orders of magnitude greater than that in the magnetic field (e.g., Finke et al. 2008; Abdo et al. 2011a,b,d,c; Aliu et al. 2013, 2014a,b). The extended jet is much closer to equipartition between electron and magnetic field density by design; a model out of equipartition would still be able to reproduce the data. These parameters are also close to previous results for modeling extended jets, although the magnetic field is a bit lower than usual (typically found $> 1 \mu\text{G}$; e.g., Tavecchio et al. 2007). This may be because previous ICCMB models of extended jets are for FSRQs, rather than BL Lac objects. One hypothesis can be that the magnetic fields in extended jets of BL Lac objects are lower than those in the extended jets of FSRQs.

It should be noted that the ICCMB model for explaining the X-ray emission from extended jets is controversial. It could be that X-rays are instead produced by synchrotron emission from another population of electrons in the extended jet (e.g., Atoyan & Dermer 2004; Hardcastle 2006). In this alternative framework, HE and VHE emission is unlikely. Recently, Meyer & Georganopoulos (2014) used *Fermi*-LAT observations to rule out the ICCMB model for the X-ray emission from the extended jet in the FSRQ 3C 273.

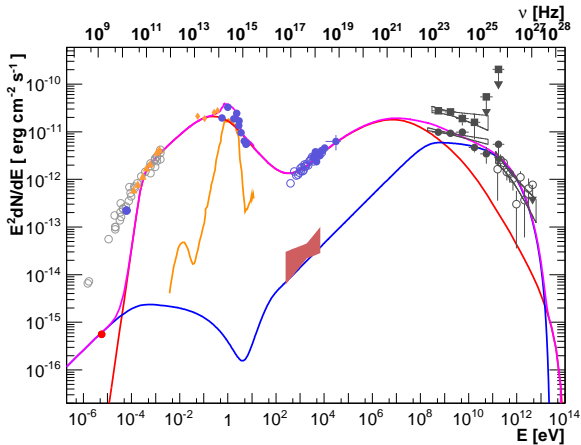
3.5 Comparison with other LBL objects

The SEDs of LBL objects detected in VHE γ -rays challenge single zone homogeneous SSC radiative models, which usually reproduce reasonably well the time-averaged SEDs of the HBL class.

The most complete simultaneous coverage of the BL Lacertae was established by Abdo et al. (2011d) during a multi-wavelength campaign including the *Fermi*-LAT and the X-ray observatories mentioned in this study for the high-energy part. The X-ray spectrum during that campaign was soft, indicating that its origin was

Table 5. Model parameters for the SED shown in Fig. 4. The redshift z is 0.049.

Parameter	Symbol	Compact component	Extended Jet
Bulk Lorentz Factor	Γ	20	8
Doppler factor	δ_D	20	8
Magnetic Field [G]	B	0.05	5.6×10^{-7}
Variability Timescale [s]	t_v	3.0×10^4	1.35×10^{11}
Comoving radius of blob [cm]	R'_b	1.7×10^{16}	3.08×10^{22}
First Electron Spectral Index	p_1	2.0	2.0
Second Electron Spectral Index	p_2	3.0	4.0
Third Electron Spectral Index	p_3	4.2	
Minimum Electron Lorentz Factor	γ'_{min}	1.0	2.0
Break Electron Lorentz Factor 1	$\gamma'_{brk,1}$	2.8×10^3	4.9×10^4
Break Electron Lorentz Factor 2	$\gamma'_{brk,2}$	6.8×10^3	
Maximum Electron Lorentz Factor	γ'_{max}	1.0×10^7	2.0×10^6
Jet Power in Magnetic Field [erg s $^{-1}$]	$P_{j,B}$	2.2×10^{42}	1.4×10^{44}
Jet Power in Electrons [erg s $^{-1}$]	$P_{j,e}$	1.7×10^{45}	2.8×10^{44}

**Figure 4.** Same as Fig. 3. The red line is the results of the SSC model from the compact component and the blue line is the flux originating from the extended jet; parameters are given in Table 5. Purple line is the sum of both.

synchrotron radiation rather than Comptonized photons, making for a wider synchrotron νF_ν distribution than is reported here for AP Librae. The difficulty in this case for modeling BL Lacertae was that the simulated SED required the energy densities to be far from equipartition. However, a 1997 *Beppo-SAX* observation (Ravasio et al. 2002) of BL Lacertae showed a clear IC origin for the X-ray radiation, yielding a narrower synchrotron distribution, for which the SSC model failed to reproduce a reasonable (non-simultaneous) HE spectrum, and an external contribution was added.

The broad Compton distribution of S5 0716+714, with emission up to ≈ 700 GeV, is either an order of magnitude *below* the best SSC model prediction from Anderhub et al. (2009), or is too wide if the *Fermi*-LAT spectrum constrains the flux at $E_{ic,peak}$ (Figure 6 in Tavecchio et al. 2010; see also the similar situation for BL Lacertae in the same Figure). Note that the HE and VHE data were not taken simultaneously in these two LBL objects.

4 CONCLUSIONS

Contemporaneous observations of AP Librae with many currently available space- and ground-based instruments have been presented. The data have revealed the broadest Compton distribution of any known blazar to date, which spans from X-ray to TeV energies.

The SED of AP Librae is difficult to reproduce with a single zone SSC model: the steep UV spectrum, probably synchrotron emission, does not connect smoothly with the X-ray spectrum, which is underestimated by an order of magnitude if a match is required with the HE γ -ray spectrum (as was also pointed out by Tavecchio et al. 2010). If a match is required with the X-rays, the *Fermi*-LAT spectrum is then largely overestimated. The new H.E.S.S. spectrum further complicates the situation, as none of the previous constraints allows this SSC model to reach the VHE domain, even assuming a predominantly Thomson scattering regime which yields Compton components roughly twice as large in νF_ν as the synchrotron component. There are ways out of the conundrum but at the cost of increased model complexity. An example is blob-in-jet model, recently proposed by Hervet et al. (2015) to reproduce the SED of Ap Librae. Another possibility is a model where electrons also upscatter soft photons originating outside of the high-energy emission site. It has been shown in this work that VHE γ rays from the extended jet, seen in X-ray, can be produced and can explain the H.E.S.S. spectrum.

AP Librae is the third of VHE detected LBL-type object for which single zone SSC models fail to reproduce the SED, and is currently the only BL Lac type object combining VHE emission and a resolved X-ray jet. The LBL class of VHE emitting objects proves to be an interesting laboratory to test radiative model scenarios, and perhaps to identify parameters on which the LBL-HBL sequence could depend.

ACKNOWLEDGEMENTS

The *Fermi* LAT Collaboration acknowledges generous ongoing support from a number of agencies and institutes that have supported both the development and the operation of the LAT as well as scientific data analysis. These include the National Aeronautics and Space Administration and the Department of Energy in the United States, the Commissariat à l'Énergie Atomique and

the Centre National de la Recherche Scientifique / Institut National de Physique Nucléaire et de Physique des Particules in France, the Agenzia Spaziale Italiana and the Istituto Nazionale di Fisica Nucleare in Italy, the Ministry of Education, Culture, Sports, Science and Technology (MEXT), High Energy Accelerator Research Organization (KEK) and Japan Aerospace Exploration Agency (JAXA) in Japan, and the K. A. Wallenberg Foundation, the Swedish Research Council and the Swedish National Space Board in Sweden.

Additional support for science analysis during the operations phase is gratefully acknowledged from the Istituto Nazionale di Astrofisica in Italy and the Centre National d'Études Spatiales in France.

This research has made use of data from the MOJAVE database that is maintained by the MOJAVE team (Lister et al. 2009). The MOJAVE program is supported under NASA-Fermi grant NNX12A087G.

The National Radio Astronomy Observatory is a facility of the National Science Foundation operated under cooperative agreement by Associated Universities, Inc.

This research has made use of the NASA/IPAC Extragalactic Database (NED) which is operated by the Jet Propulsion Laboratory, California Institute of Technology, under contract with the National Aeronautics and Space Administration.

This publication makes use of data products from the Wide-field Infrared Survey Explorer, which is a joint project of the University of California, Los Angeles, and the Jet Propulsion Laboratory/California Institute of Technology, funded by the National Aeronautics and Space Administration.

The authors want to acknowledge C.C. Cheung for the VLA radio observation used for contours presented in Figure 2. A.S. acknowledges useful discussions with Dan Harris on the problematics of *Chandra* data analyses. We thank the Swift and *RXTE* teams for their cooperation in joint observations of AP Librae. This research has made use of data provided by the SIMBAD database, operated at CDS, Strasbourg, France.

D.S. was partially supported by the Labex ENIGMASS

YYK and ABP were supported in part by the Russian Foundation for Basic Research (project 13-02-12103)

TS was partly supported by the Academy of Finland project 274477.

REFERENCES

- Abdo, A. A., et al. 2010, *ApJ*, 716, 30
 —. 2011a, *ApJ*, 736, 131
 —. 2011b, *ApJ*, 727, 129
 —. 2011c, *ApJ*, 726, 43
 —. 2011d, *ApJ*, 730, 101
 Abramowski, A., et al. 2015, *A&A*, 573, A31
 Ackermann, M., et al. 2011, *ApJ*, 743, 171
 Aharonian, F., et al. 2006, *Nature*, 440, 1018
 —. 2007, *A&A*, 470, 475
 Albert, J., et al. 2007, *ApJL*, 666, L17
 Aliu, E., et al. 2013, *ApJ*, 779, 92
 —. 2014a, *ApJ*, 782, 13
 —. 2014b, *ApJ*, 797, 89
 Anderhub, H., et al. 2009, *ApJL*, 704, L129
 Arnaud, K. A. 1996, in *Astronomical Society of the Pacific Conference Series*, Vol. 101, *Astronomical Data Analysis Software and Systems V*, ed. G. H. Jacoby & J. Barnes, 17–+
- Atayan, A., & Dermer, C. D. 2004, *ApJ*, 613, 151
 Band, D. L., & Grindlay, J. E. 1985, *ApJ*, 298, 128
 Bessell, M. S. 1990, *PASP*, 102, 1181
 Błażejowski, M., Sikora, M., Moderski, R., & Madejski, G. M. 2000, *ApJ*, 545, 107
 Bonning, E., et al. 2012, *The Astrophysical Journal*, 756, 13
 Böttcher, M., Dermer, C. D., & Finke, J. D. 2008, *ApJL*, 679, L9
 Breeveld, A. A., Landsman, W., Holland, S. T., Roming, P., Kuin, N. P. M., & Page, M. J. 2011, in *American Institute of Physics Conference Series*, Vol. 1358, *American Institute of Physics Conference Series*, ed. J. E. McEnery, J. L. Racusin, & N. Gehrels, 373–376
 Burrows, D. N., et al. 2005, *Space Sci. Rev.*, 120, 165
 Cardelli, J. A., Clayton, G. C., & Mathis, J. S. 1989, *ApJ*, 345, 245
 Celotti, A., Ghisellini, G., & Chiaberge, M. 2001, *MNRAS*, 321, L1
 Davis, J. E. 2001, *ApJ*, 562, 575
 Falomo, R., Bersanelli, M., Bouchet, P., & Tanzi, E. G. 1993, *AJ*, 106, 11
 Finke, J. D., Dermer, C. D., & Böttcher, M. 2008, *ApJ*, 686, 181
 Franceschini, A., Rodighiero, G., & Vaccari, M. 2008, *A&A*, 487, 837
 Godet, O., et al. 2009, *A&A*, 494, 775
 Hardcastle, M. J. 2006, *MNRAS*, 366, 1465
 Harris, D. E., et al. 2011, *ApJ*, 743, 177
 Hervet, O., Boisson, C., & Sol, H. 2015, *ArXiv e-prints*
 Hofmann, W. 2010, *The Astronomer's Telegram*, 2743, 1
 Hyvönen, T., Kotilainen, J. K., Falomo, R., Örndahl, E., & Pursimo, T. 2007, *A&A*, 476, 723
 Jahoda, K., Swank, J. H., Giles, A. B., Stark, M. J., Strohmayer, T., Zhang, W., & Morgan, E. H. 1996, in *Society of Photo-Optical Instrumentation Engineers (SPIE) Conference Series*, Vol. 2808, *Society of Photo-Optical Instrumentation Engineers (SPIE) Conference Series*, ed. O. H. Siegmund & M. A. Gummin, 59–70
 Jones, D. H., et al. 2009, *MNRAS*, 399, 683
 Jones, F. C. 1968, *Physical Review*, 167, 1159
 Kalberla, P. M. W., Burton, W. B., Hartmann, D., Arnal, E. M., Bajaja, E., Morras, R., & Pöppel, W. G. L. 2005, *A&A*, 440, 775
 Kaufmann, S., Wagner, S. J., & Tibolla, O. 2013, *ApJ*, 776, 68
 Lister, M. L., Marscher, A. P., & Gear, W. K. 1998, *ApJ*, 504, 702
 Lister, M. L., et al. 2009, *AJ*, 137, 3718
 —. 2013, *AJ*, 146, 120
 Meyer, E. T., & Georganopoulos, M. 2014, *ApJL*, 780, L27
 Nolan, P. L., et al. 2012, *ApJS*, 199, 31
 Padovani, P., & Giommi, P. 1995, *ApJ*, 444, 567
 Paggi, A., Massaro, F., Vittorini, V., Cavaliere, A., D'Ammando, F., Vagnetti, F., & Tavani, M. 2009, *A&A*, 504, 821
 Planck Collaboration et al. 2011, *A&A*, 536, A7
 Poole, T. S., et al. 2008, *MNRAS*, 383, 627
 Ravasio, M., et al. 2002, *A&A*, 383, 763
 Roming, P. W. A., et al. 2009, *ApJ*, 690, 163
 Sambruna, R. M., Gambill, J. K., Maraschi, L., Tavecchio, F., Cerutti, R., Cheung, C. C., Urry, C. M., & Chartas, G. 2004, *ApJ*, 608, 698
 Sanchez, D. A., Fegan, S., & Giebels, B. 2013, *ArXiv e-prints*
 Schlafly, E. F., & Finkbeiner, D. P. 2011, *ApJ*, 737, 103
 Shaw, M. S., et al. 2013, *The Astrophysical Journal*, 764, 135
 Sikora, M., Begelman, M. C., & Rees, M. J. 1994, *ApJ*, 421, 153
 Silva, L., Granato, G. L., Bressan, A., & Danese, L. 1998, *ApJ*, 509, 103

- Tavecchio, F., Ghisellini, G., Ghirlanda, G., Foschini, L., & Maraschi, L. 2010, MNRAS, 401, 1570
- Tavecchio, F., Maraschi, L., & Ghisellini, G. 1998, ApJ, 509, 608
- Tavecchio, F., Maraschi, L., Sambruna, R. M., & Urry, C. M. 2000, ApJL, 544, L23
- Tavecchio, F., Maraschi, L., Wolter, A., Cheung, C. C., Sambruna, R. M., & Urry, C. M. 2007, ApJ, 662, 900
- The Fermi-LAT Collaboration. 2013, ArXiv e-prints 1306.6772
- Tsujimoto, M., et al. 2011, A&A, 525, A25
- Vaughan, S., Edelson, R., Warwick, R. S., & Uttley, P. 2003, MNRAS, 345, 1271
- Wright, E. L. 2006, PASP, 118, 1711
- Wright, E. L., et al. 2010, AJ, 140, 1868
- Zensus, J. A., Ros, E., Kellermann, K. I., Cohen, M. H., Vermeulen, R. C., & Kadler, M. 2002, AJ, 124, 662

APPENDIX A: CONSTRAINTS FOR AN ARBITRARY FIELD OF SEED PHOTONS

In leptonic class models, the inverse Compton process is responsible for the high energy part of the SED. The seed photons originate either from synchrotron radiation produced within the jet (SSC models) or from a source outside of the jet (external Compton models). In the latter case, the sources can be either the broad-line regions or the dust torus (Sikora et al. 1994; Błażejowski et al. 2000).

The peak observed energy E_s of an electron with Lorentz factor γ is given by

$$E_s/m_e c^2 = \frac{\delta \gamma^2 B}{(1+z)B_{cr}},$$

and the Compton-scattered photon energy by

$$E_{ic}/m_e c^2 = \frac{\delta \gamma^2 \epsilon'_{seed}}{(1+z)},$$

where the energy⁷ of the seed photons is ϵ_{seed} (respectively $\epsilon'_{seed} = \delta \epsilon_{seed}$ in the jet's frame).

Efficient Compton scattering will occur only for electrons below the KN limit:

$$\gamma \leq (4\epsilon'_{seed})^{-1}. \quad (\text{A1})$$

This KN limit means that Compton-scattered photons will be mainly restricted to energies:

$$E_{ic}/m_e c^2 \leq \frac{\delta}{16(1+z)\epsilon'_{seed}}.$$

The synchrotron photons produced by the electrons having the energy $(4\epsilon'_{seed})^{-1}$ have a peak energy given by:

$$E_s/m_e c^2 = \frac{\delta B}{16(1+z)\epsilon'^2_{seed} B_{cr}}.$$

Combining the last two equations with the constraints on maximal values for $E_s \approx 0.1$ keV and $E_{ic} \approx 1$ TeV derived from the observations yields:

$$\frac{\delta}{70} \geq \frac{B}{10^{-2}G}, \quad (\text{A2})$$

which requires either an unusually high Doppler factor, or an unusually low magnetic field. If the 1 TeV photons are produced by IC scattering in the KN regime, Eq. A1 becomes

$$\gamma \geq (4\epsilon'_{seed})^{-1}$$

and the observed photon energy is (Tavecchio et al. 1998)

$$E_c/m_e c^2 = \frac{\delta \gamma}{(1+z)}.$$

Then Eq. A2 reads

$$\frac{\delta}{17.5} \leq \frac{B}{10^{-2}G} \quad (\text{A3})$$

which is a reasonable constraint. Note that this calculation applies no matter what the seed photon source is (broad-line region or dust torus or synchrotron photons produced within the jet), illustrating the difficulties of either radiative scenarios to account for the main SED features of AP Librae in the Thomson regime.

APPENDIX B: CANDIDATES FOR VHE OBSERVATIONS

The detection of AP Librae by the H.E.S.S. telescopes has revealed the broadest IC component for a blazar with a peak position at very low energy. Unfortunately, only a handful of LBL-type objects have yet been detected at VHEs. To decide if AP Librae is a special case or a typical representative of the LBL class, other LBL objects have to be observed by Čerenkov telescope and detected at VHE.

Due to their limited field of view (≈ 5 deg), an extra-galactic survey performed by Čerenkov telescopes is not possible yet. As a consequence, good targets for observations have to be found based on multi-wavelengths data. In this appendix, six LBL-type objects, present in the second catalog of *Fermi* sources (2FGL, Nolan et al. 2012) were selected based on their possible VHE emission. The 2FGL best fit power-law, measured in the 100 MeV-100 GeV band, was extrapolated above 200 GeV and EBL correction was made based on the Franceschini et al. (2008) model. The redshift information was extracted either from the second catalog of AGN (2LAC, Ackermann et al. 2011) or from Shaw et al. (2013). Sources without redshift measurement were excluded and only sources classified as a BL Lac of the LBL class were retained. Note that AP Librae appeared to be the first on this list when building it.

The names of six candidates, ranked by predicted flux above 200 GeV, are given in Table B1. For illustration, their SEDs, built from archival data using the ASDC SED builder⁸, are presented in Figure B1. Two out of the six sources can be observed by H.E.S.S. and five by the northern facilities (VERITAS and MAGIC). Despite its location and with a redshift of $z = 0.424$, the source 2FGL J0738.0+1742 can be well suited for H.E.S.S. II telescope observations given the lower energy threshold (50 GeV) of the instrument. The redshifts of 2FGL J1150.1+2419 and 2FGL J1150.1+2419, found in the 2LAC, were not confirmed by Shaw et al. (2013). Five out of 6 are also present in the first Fermi-LAT Catalog of Sources Above 10 GeV (1FHL, The Fermi-LAT Collaboration 2013, see Figure B1).

⁷ The notation $E = \epsilon m_e c^2$ is adopted here.

⁸ <http://tools.asdc.asi.it/SED/>

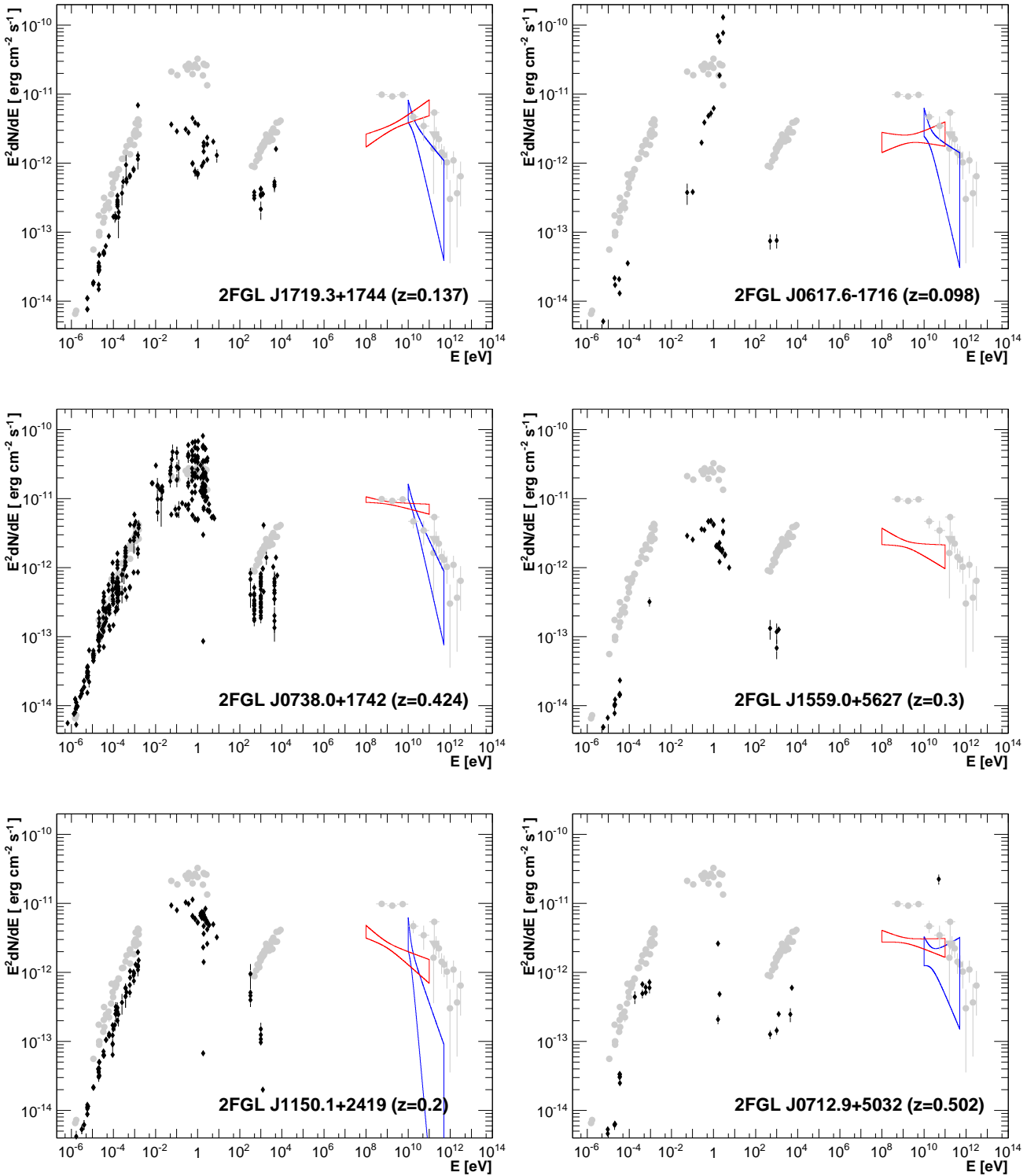


Figure B1. SEDs for the six LBL objects selected. The black points are archival data while the respectively red and blue butterflies are the 2FGL and 1FHL measurements. Gray points are the AP Librae data presented in this work.

Table B1. Proposed LBL-type objects for VHE observations. The 2FGL name is given in the first column with the position in the second and third. The redshift measurement taken from (Ackermann et al. 2011) or (Shaw et al. 2013) is reported in the fourth column. The name (column 5) of the counterpart associated with the 2FGL source was found in the 2LAC catalog. The last column in the mane of the best suited instrument for observations. The sources are ranked by predicted flux above 200 GeV.

2FGL name	α_{J2000}	δ_{J2000}	redshift	Association	Instruments
2FGL J1719.3+1744	17 ^h 19 ^m 13.05 ^s	17° 45' 06.4''	0.137	PKS 1717+177	VERITAS/MAGIC
2FGL J0617.6-1716	06 ^h 17 ^m 33.67 ^s	-17° 15' 22.8''	0.098	CRATES J061733.67-171522.8	H.E.S.S.
2FGL J0738.0+1742	07 ^h 38 ^m 07.39 ^s	17° 42' 19.0''	0.424	PKS 0735+17	VERITAS/MAGIC - H.E.S.S.
2FGL J1559.0+5627	15 ^h 58 ^m 48.29 ^s	56° 25' 14.1''	0.3	TXS 1557+565	VERITAS/MAGIC
2FGL J1150.1+2419	11 ^h 50 ^m 19.21 ^s	24° 17' 53.8''	0.2	B2 1147+24	VERITAS/MAGIC
2FGL J0712.9+5032	07 ^h 12 ^m 43.68 ^s	50° 33' 22.7''	0.502	GB6 J0712+5033	VERITAS/MAGIC